

INVESTIGATION OF OFF-DESIGN CONDITIONS IN A RADIAL PUMP BY USING TIME-RESOLVED-PIV

Nico Krause¹, Elemér Pap², Dominique Thévenin³

1: Laboratory of Fluid Dynamics and Technical Flows, University of Magdeburg "Otto von Guericke", Magdeburg, Germany, Nico.Krause@vst.uni-magdeburg.de

2: Elemer.Pap@vst.uni-magdeburg.de

3: Dominique.Thevenin@vst.uni-magdeburg.de

Abstract In industrial applications turbomachines are not only used at their design point, but also at significant lower or higher flow rates. This operating range is limited on the low flow rate side by instabilities in flow-leading parts of the machinery. For these operating conditions vortices are created due to the separation of the boundary layer from the walls of the flow-leading parts of the machine, e. g. in the impeller. These unique or multiple stall cells can start to propagate at a fraction of the rotor speed in the impeller when the flow is further throttled. They induce very strong pressure oscillations and as a result machine parts can even be destroyed. It is very difficult to describe these phenomena physically and especially mathematically, because they depend on many operational parameters of the considered turbomachine. In the present experimental set-up a radial pump is investigated for various operating conditions down to rotating stall. To investigate the flow field in every channel of the impeller Time-Resolved PIV is used, so that measurements in transient and unsteady flows inside the rotating system become possible. In this study acquisition frequencies of 50 Hz, 500 Hz and 800 Hz are used with a 1280x1024 pixel CMOS-camera. For a frequency of 50 Hz a measuring series consists of 500 double pictures. This means that it is possible to measure the flow field over 100 rotations of the impeller. These measurements are used to calculate the frequency of the stall cell. The higher acquisition frequencies are used to investigate and characterise in more details the flow field in the impeller. The flow field is measured in each channel of the impeller at the same position. In order to determine the circumferential speed of the rotating stall in the impeller a frequency analysis is applied to the measured flow field. For this, each individual velocity vector in the flow field is analyzed using FFT both for the direction and the magnitude of the vector. To obtain a characteristic frequency spectrum of the flow field the mean value is then obtained through averaging of the separate frequency spectra for each vector. The oscillation frequency of the flow field and thus the displacement speed of the rotating stall cell can be determined in that way from the measured velocity fields.

1. Introduction

In many applications pumps are not used at the design point. Wurm (2004) indicates that in head installations over 50% of the time pumps operate at under 25% of the design flow rate. In such cases the pump operates under part-load flow and the inflow condition differs from the dimensioning point.

For turbomachines operating with gases the problem of rotating stall has been known for a long time. The first description was given by Emmons et al. (1955). In turbomachines there exists a classical velocity triangle with the components \underline{c} (absolute velocity), \underline{u} (peripheral velocity) and \underline{w} (relative velocity) (Eq. 1, Fig. 1a).

$$\underline{c} = \underline{u} + \underline{w} \tag{1}$$

If the flow rate is reduced, the meridian component of the relative velocity w_m also decreases (Fig. 1b). For this reduced flow rate the angle of attack rises and the stagnation point is displaced to the pressure side of the blade. When the angle of attack exceeds a certain threshold, the flow on the suction side will detach and stall can appear.

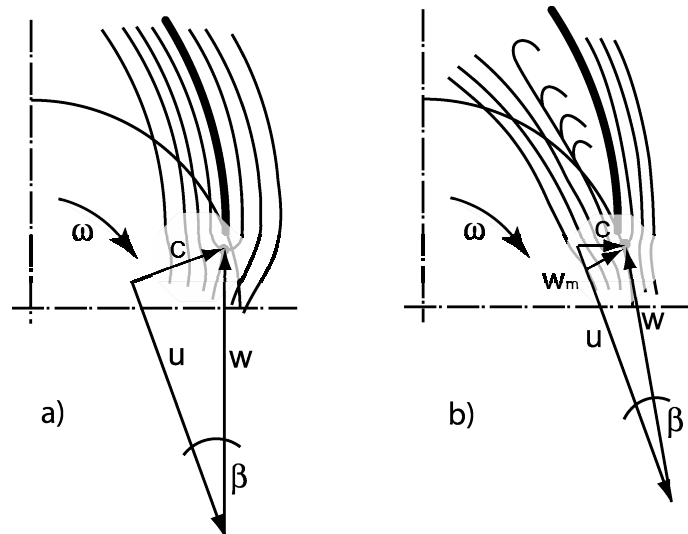


Fig. 1 a-b. Velocity triangles at design point (a) and for throttled flow (b)

The static pressure inside the stall region is smaller than in the surrounding flow. Vortices can therefore appear with the same rotating direction as the impeller. In the outlet of the blade passage a second vortex can be formed with an inverse rotational direction. These vortices can grow until the complete blade passage is blocked. Then, the medium has to pass through the following channel. This leads once more to a displacement of the stagnation point in the following blade passage, and a new stall cell will be formed in this channel. On the other hand, the flow in the first blade passage will reattach and the flow conditions in this channel will improve. With this mechanism the stall cell(s) can turn around through the impeller. Because the angular velocity of the stall cell is lower than the impeller angular velocity, it turns inside the impeller against the rotational direction. It is furthermore possible that several stall cells exist simultaneously in the impeller.

Rotating stall leads to considerable efficiency losses. Many studies have investigated this phenomenon, mostly in axial compressors (Bently et al. 2001, Inoue et al. 2000, Walbaum 1999). Pampreen (1993) gives an extensive review of this problem. A limitation of all these studies is that they are based on high frequency single-point measurements of pressure (Dobat et al. 2001, Escuret and Garnier 1996, Garnier et al. 1991, Höss et al. 2000, Saxer-Felici et al. 1999, Surek 2001) temperature or velocity (Day 1993, Garnier et al. 1991, Place et al. 1996, Walbaum 1999) obtained through intrusive diagnostics, or on very low frequency non-intrusive imaging techniques (Wernet et al. 2001). But, for such instabilities, intrusive measurements can easily falsify the results. A first investigation relying on a high frequency non-intrusive imaging technique was presented by Krause et al. (2005).

In the present study, velocity fields measured in a centrifugal pump with time-resolved PIV at high frame rates are presented. These measurements concerning instabilities and turbulent processes clearly show rotating stall in a throttled radial water pump with different blade designs.

2. EXPERIMENTAL SET-UP

The set-up used in the experiments consists in two major parts: the Time-resolved PIV system and the rotating machinery installation. Fig. 2 shows a sketch of this installation, where the pipes and the acryl model pump can be distinguished.

2.1. Radial pump

The investigated transparent radial pump is situated in a water circuit. An inductive flow meter measures the volume flow, which can be adjusted by a hand valve in the pressure pipe. Pressure probes in the suction pipe and after the impeller, shown in Fig. 3, measure the static pressure before the pump and the pressure difference over the impeller. With these components it is possible to get reproducible operating points. A meridian section of the pump is presented in Fig. 4.

For the design of pump blades different concepts are used. The inlet and outlet angles are given by the needed pressure difference and remain the same for all geometries.

Table 1. Technical parameters of the radial pump

Q_d	47	[m ³ /h]	Flow rate at design point	r_1	65	[mm]	Inlet radius
n	600	[min ⁻¹]	Number of revolutions	r_2	139	[mm]	Outlet radius
β_1	19	[°]	Inlet angle	n_q	26	[min ⁻¹]	Specific speed
β_2	23	[°]	Outlet angle				

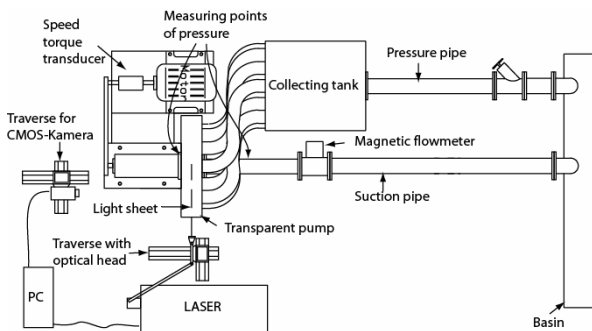


Fig. 2 Sketch of the radial transparent pump installation with PIV measurement system.

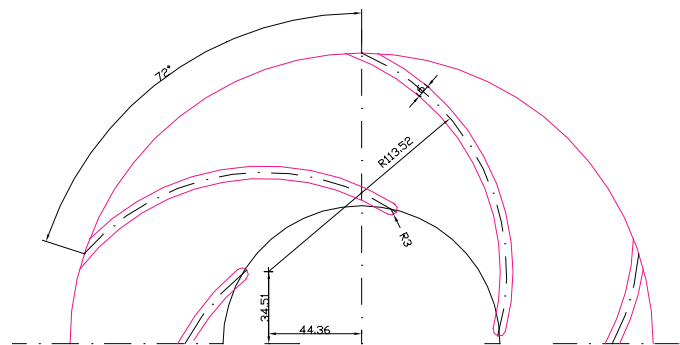


Fig. 3 Geometry of the impeller.

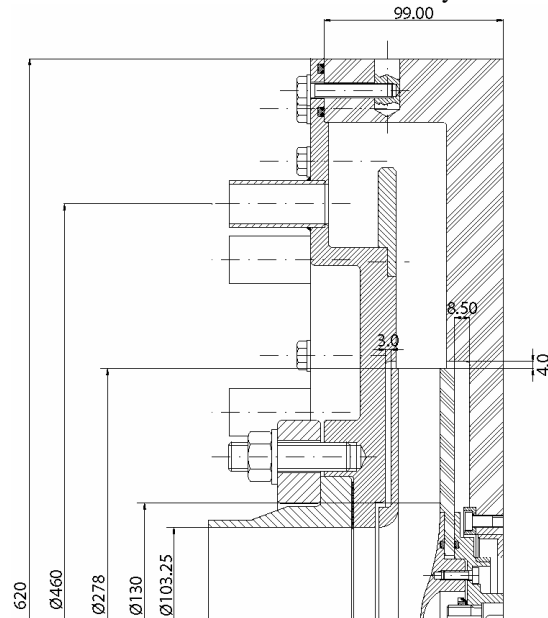


Fig. 4 Meridian section of the pump.

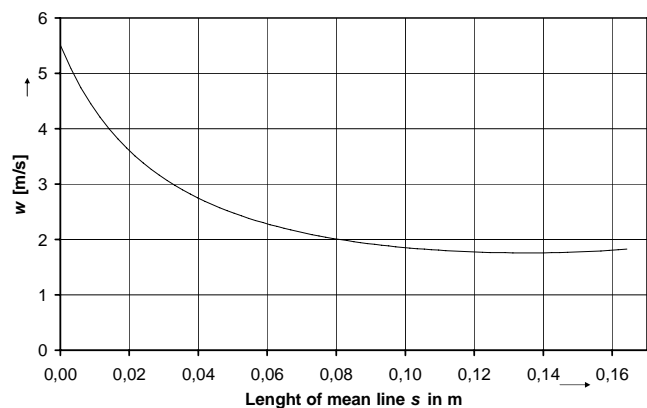


Fig. 5 Relative velocity over the mean line of the blade at the design point.

One simple concept is a blade geometry given by one circular arc with a single radius. The advantages are: short length of the mean line, small hydraulic losses and simple structure. The disadvantage is the fast deceleration of the flow in the first third of the blade passage and

acceleration near the outlet. The corresponding geometry is presented in Fig. 3 and is retained in the present study. Fig. 5 shows the relative velocity over the mean line for the design point where the fast deceleration of the flow in the first third of the blade passage is visible. Technical parameters are listed in Table 1.

2.2. Measuring system

For the velocity measurements a commercial Time-resolved PIV system from DantecDynamics A/S is used. The principles of PIV are described e.g. by Willert and Gharib (1991). The TR-PIV-system is composed of a Q-switched Nd:YAG laser, laser-sheet optics, a CMOS double-image camera, a synchronisation unit and the control, acquisition and treatment computer. The frequency-doubled, diode-pumped Nd:YAG laser has a variable repetition rate, allowing pulse intervals from 40 to 1000 μ s, with a pulse duration of 75-250 ns. The pulse energy strongly depends on the repetition rate with a maximum energy of about 22 mJ at lower repetition rates. The light sheet optics have been adjusted in order to get a diverging light sheet of 0.5-1 mm thickness inside the pump. The PIV images were taken with a 1260x1024 pixel, 10 bit CMOS camera, working with frame rates up to 500 image pairs/s full frame and 800 images pairs/s with 1260x640 pixels. For the investigation frequencies of 50 and 800 Hz have been used. The frequency of 50 Hz corresponds to a measurement of each blade of the impeller in a fixed position. To follow the vortices within one channel the higher frequency is used. The seeding material consists in Rhodamin-B-doped PMMA-particles with a mean size of 10 μ m and a density $\rho=1,19$ kg/dm³.

To measure the static pressure rise the pressure before the impeller in the suction side and after the impeller at $r=160$ mm was recorded. The velocity energy after the impeller at the same radius is calculated from the PIV-data.

3. Results

3.1 Pump characteristic

Fig. 6 shows the static pressure rise over the flow rate coefficient Q/Q_0 (Q_0 : design flow rate) for the impeller (Δp_{stat}). This is not the complete energy transmission to the fluid because the velocity term is missing (Eq. 2).

$$\Delta p_{ges} = \Delta p_{stat} + \frac{\rho}{2}(c_2^2 - c_1^2) \quad (2)$$

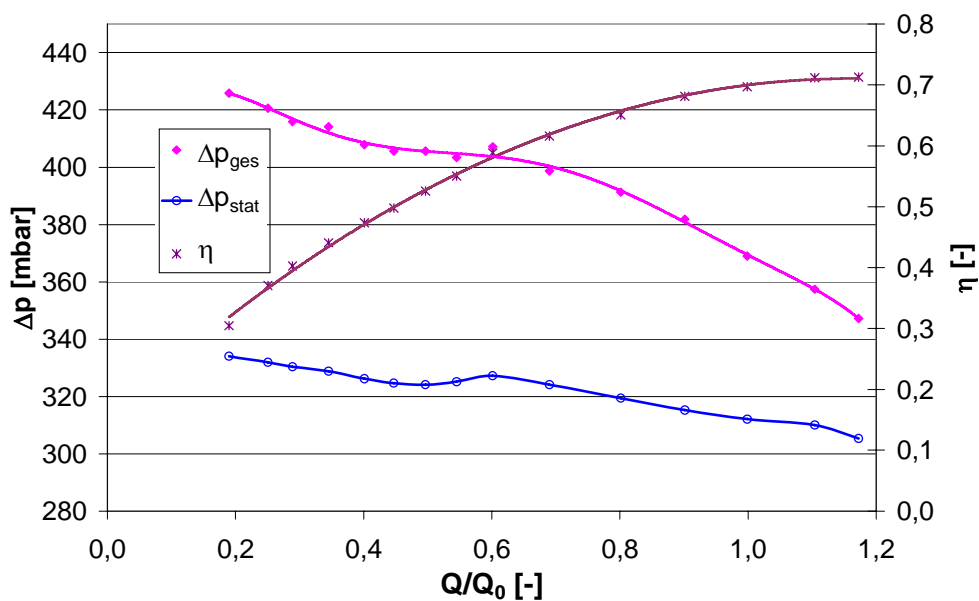


Fig. 6 Pump characteristic curve

In the diagram the complete energy transmission is also shown as Δp_{ges} , where the velocity term is added by post-processing the PIV data. With the data from the speed torque transducer the efficiency can be calculated (Eq. 3) using M , the speed torque and ω , the angular velocity. The reaction degree (Eq. 4) equals $\Re=0.7$ at the design point and depends on the flow rate. The static pressure difference decreases slightly below $Q/Q_0=0.6$ towards lower flow rates (Fig. 6). This is due to the fact that, in this part of the characteristic curve a stall cell appears in two channels of the impeller. The position of the standing stall depends on the exact blade geometry, which is not perfectly rotationally symmetric.

$$\eta = \frac{\Delta p_{ges} \cdot Q}{M \cdot \omega} \quad (3)$$

$$\Re = \frac{e_{u(stat)}}{e_{u(stat)} + e_{u(kin)}} \quad (4)$$

3.1. Part-load flow

The measured flow fields are analysed with Fast-Fourier-Transform (FFT). For this purpose one visible part of the blade passage has been selected, typically the inlet region of a channel. The procedure is similar to that presented in Krause et al. (2005). The examined flow rates are 50% to 20% of the design flow rate in steps of 5%. The onset of rotating stall could be observed at 35% of the design flow-rate. Two stall cells have been identified, propagating with a fraction of the impeller speed. The result of the FFT-analysis is presented in Fig. 7, based only on data obtained from a single channel always observed at the same position, leading to an equivalent sampling rate of 10 Hz. The maximum in the FFT-results is at a frequency of 1.3 Hz (and its harmonic 2.6 Hz), which corresponds to 7.6 rotations of the impeller before finding again the stall cell in the same position.

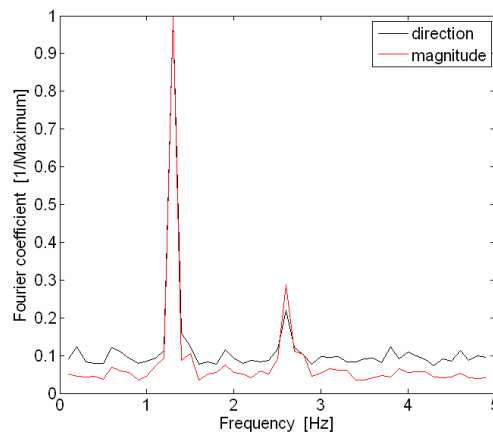


Fig. 7. Frequency spectra at 25% of the design flow rate

3.1.1 Part-load flow of 25%

As an example of the development of a stall cell in a channel eight Figures at 25% of the design flow rate are now presented. Two pictures separated by a time distance of $\Delta t=3.375$ ms (corresponding to the acquisition frequency of 800 Hz) are presented in Figures 8 to 11 in order to illustrate the typical time-evolution of the flow field. The experimentally measured flow fields are rotated in the post-processing so that all channels always appear at the same position. The coloration displays the meridian component of the relative velocity (w_m in m/s, see colour scale) and characterise thereby the discharge through the channel. The instantaneous stream lines obtained from the two-dimensional velocity field measurements are also represented.

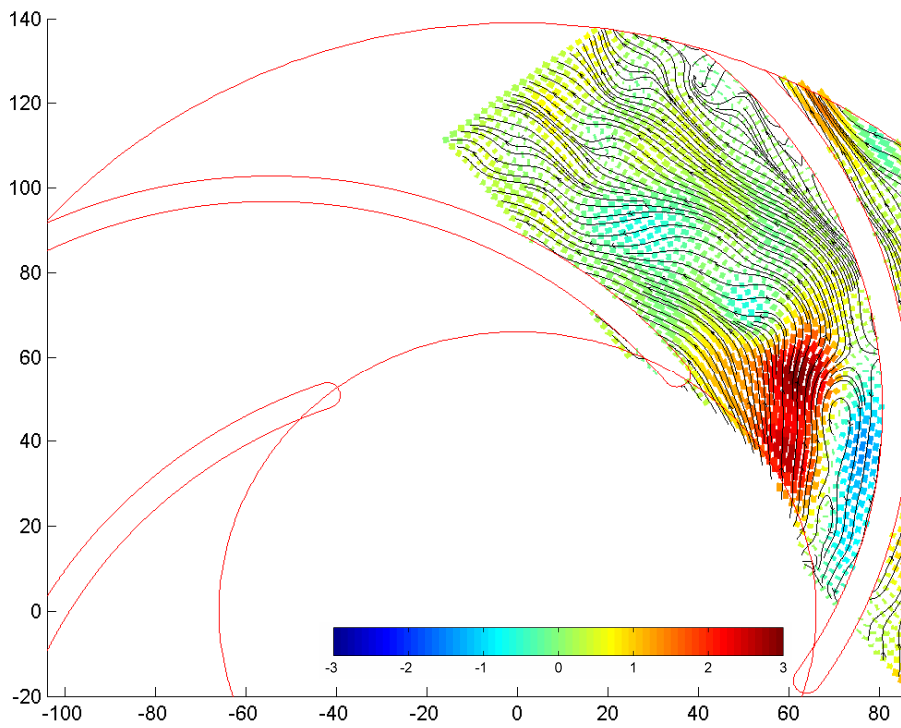
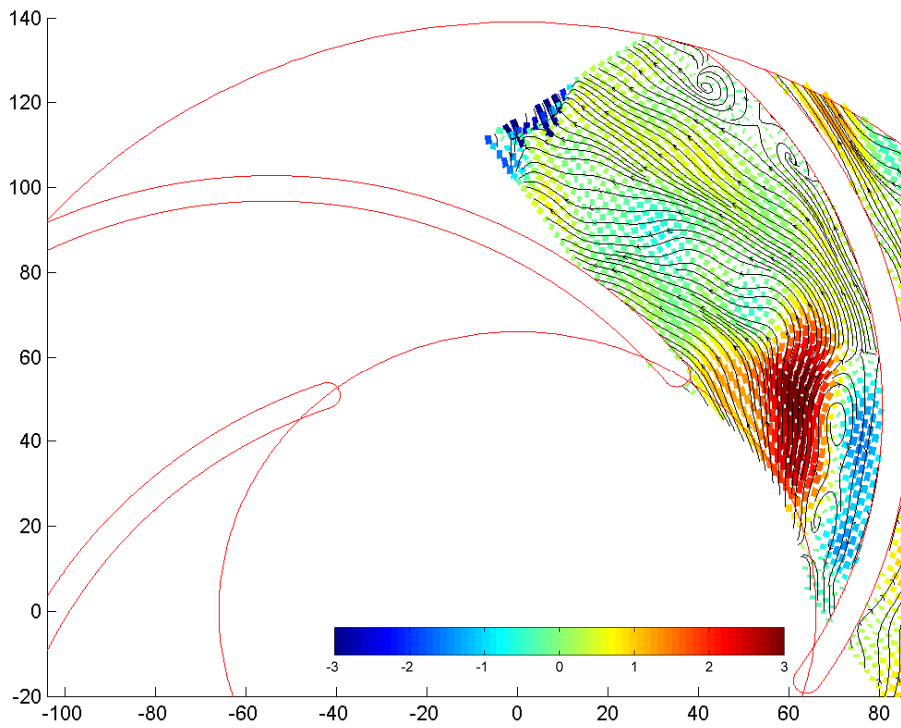


Fig. 8 Beginning of a stall cell and vortex creation

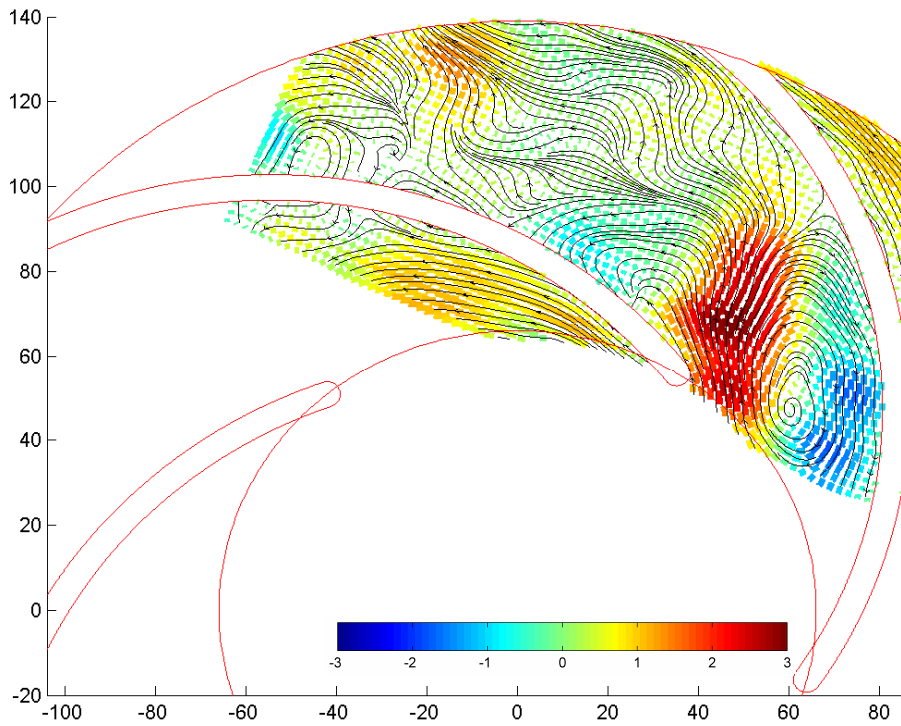
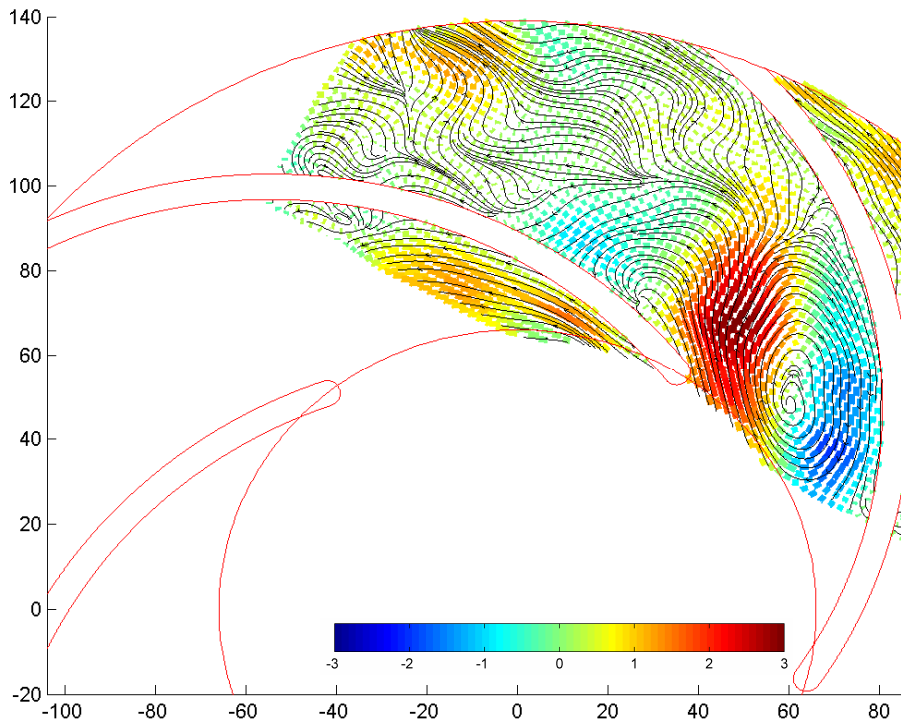


Fig. 9 Vortex at the inlet of the blade passage and low discharge

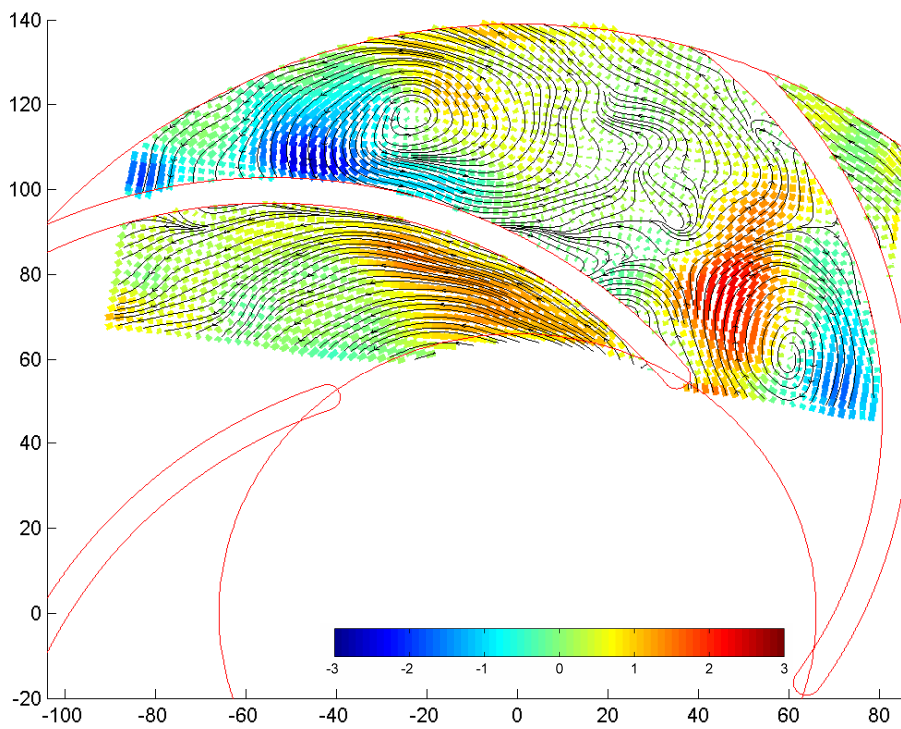
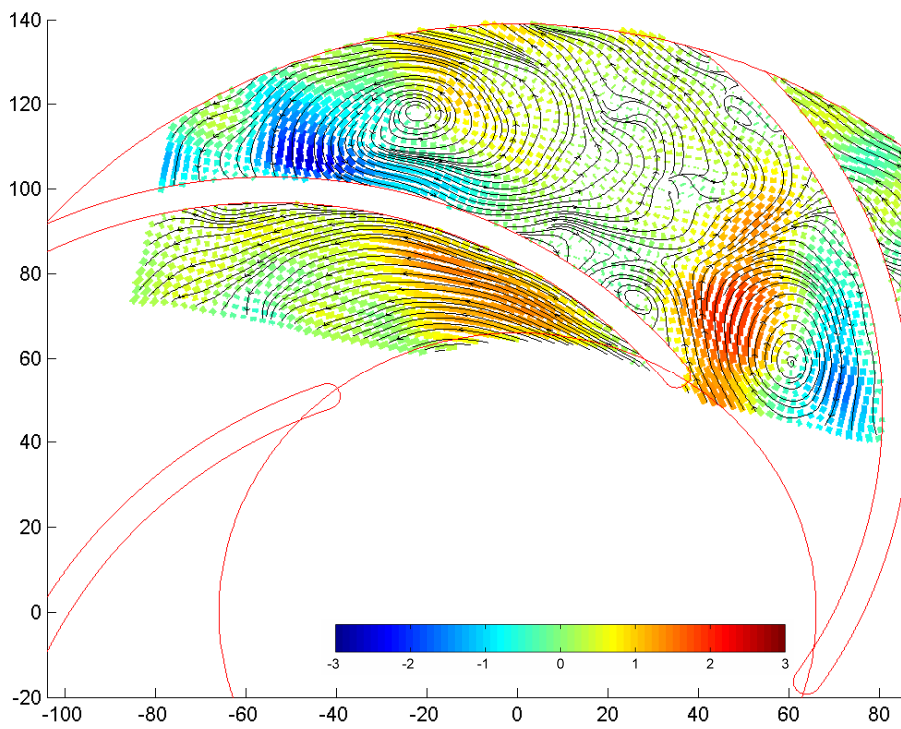


Fig. 10 Blockage of the blade passage by two strong vortices

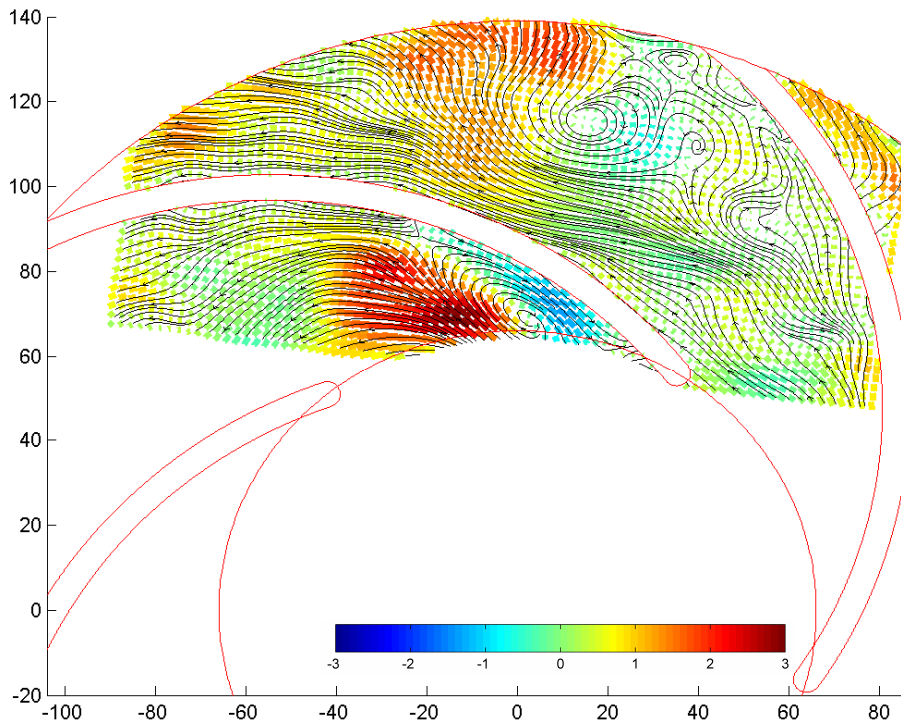
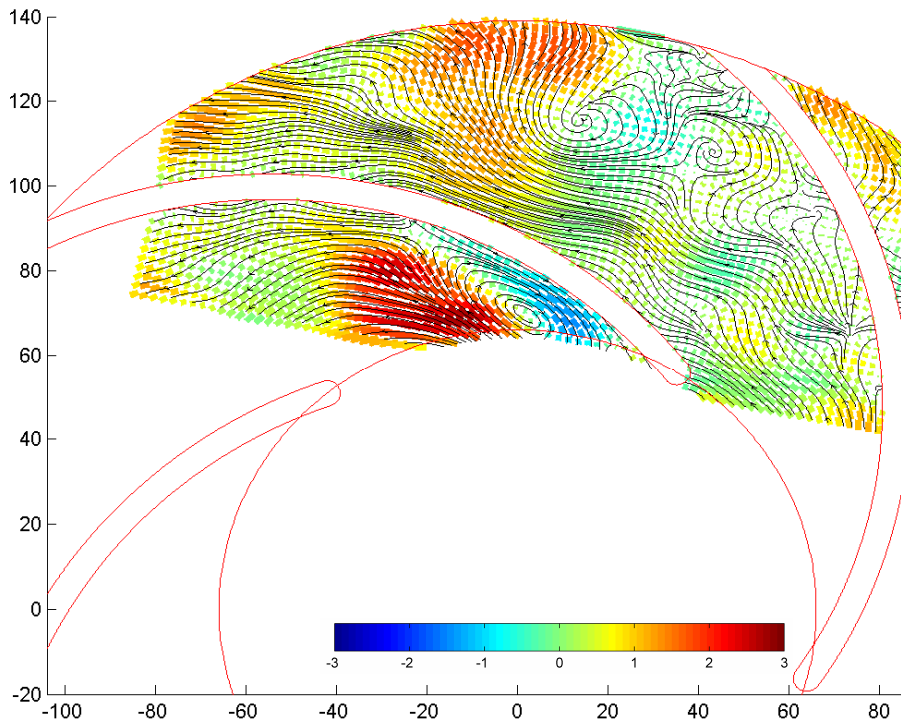


Fig. 11 End of the blockage with a small vortex at the outlet

The first image pair (Fig. 8) shows the beginning of a stall cell. The flow separates from the suction side of the blade and a vortex is created. In the first step the flow can not follow the blade in this region and a chaotic flow is visible. From this conditions small vortices are first created (they are still visible near the outlet of the channel on the suction side) before a large vortex is created from this disturbance. This vortex grows up until the inlet of the channel is partly blocked (Fig. 9). In this figure it is also visible that the transport component becomes lower. The energy transmission between the impeller and the fluid is thus reduced. The flow in the radial vaneless diffuser behind the blocked channel has more energy. This consequence, combined with the vortex at the channel inlet further leads to a blockage of the blade passage. In the blocked channel the fluid near the outlet is associated with a lower energy. This fluid region can therefore easily be entrained by both sides through viscosity and begins also to rotate (Fig 10). The direction of the rotation of this vortex is opposite from the vortex at the inlet. The inlet vortex later on moves in the flow direction, towards the outlet (Fig. 11). The viscous interaction between this vortex and the surrounding fluid finally leads to energy loss of the vortex and as a result the vortex will remain near the outlet with a decreasing size. It has never been observed that the vortex would be transported out of the channel and inside the radial vaneless diffuser.

4. Summary

Time-resolved PIV measurements have been used to determine the velocity fields in a rotating radial pump impeller. By the use of this method it is possible to capture unsteady flow phenomena appearing in the impeller at throttled flow rates. A rotating stall cell has been observed and the evolution of the time-dependent flow field has been characterised. A FFT-analysis is used to obtain the circumferential speed of the stall cell and shows that the speed of the impeller and that of the stall cell increasingly differ when the flow-rate is reduced.

REFERENCES

- Bently DE, Goldman P, Yuan J (2001) Rotor Dynamics of Centrifugal Compressors in Rotating Stall. *Orbit*, 22, pp. 40-50
- Day IJ (1993) Stall inception in axial flow compressors. *J Turbomachinery*, 115, pp. 1-9
- Dobat A, Saathoff H, Wulff D. (2001). Experimentelle Untersuchungen zur Entstehung von Rotating Stall in Axialventilatoren. *Proc. Ventilatoren: Entwicklung - Planung - Betrieb*, Braunschweig, Germany
- Emmons HW, Pearson CE, Grant HP (1955) Compressor surge and stall propagation. *Trans. of ASME*, 79, pp. 455-469
- Escuret JF, Garnier V (1996) Stall inception measurements in a high-speed multistage compressor. *J Turbomachinery*, 118, pp. 690-696
- Garnier VH, Epstein AH, Greitzer EM (1991) Rotating waves as a stall inception indication in axial compressors. *J Turbomachinery*, 113, pp. 290-302
- Höss B, Leinhos D, Fottner L (2000) Stall inception in the compressor system of a turbofan engine. *J Turbomachinery*, 122, pp. 32-44
- Inoue M, Kuromaru M, Tanino T, Furukawa M (2000) Propagation of multiple short-length-scale stall cells in an axial compressor rotor. *J Turbomachinery*, 122, pp. 45-54

- Krause N, Zähringer K, Pap E (2005) Time-Resolved Particle Imaging Velocimetry for the Investigation of Rotating Stall in a Radial Pump. *Exp Fluids*, 39, pp. 192 - 201
- Pampreen RC (1993) Compressor surge and stall. Norwich, Vt.: Concepts ETI
- Place JMM, Howard MA, Cumpsty NA (1996) Simulating the multistage environment for single-stage compressor experiments. *J Turbomachinery*, 118, pp. 706-716
- Saxer-Felici HM, Saxer AP, Inderbitzin A, Gyarmathy G. (1999). Structure and propagation of rotating stall in a single- and a multi-stage axial compressor. Proc. International Gas Turbine and Aeroengine Congress and Exhibition, Indianapolis, Indiana, USA
- Surek D (2001) Kombination von Radial- und Seitenkanalstufen für Turboverdichter. *Forschung im Ingenieurwesen*, 66, pp. 193-210
- Walbaum M (1999) Entstehungsmechanismen und Erscheinungsformen des Rotating Stall in einem sechsstufigen Axialverdichter mit verstellbaren Leitschaufeln. Düsseldorf: VDI Verl. 128
- Wernet MP, Bright MM, Skoch GJ (2001) An investigation of surge in a high-speed centrifugal compressor using digital PIV. *J Turbomachinery*, 123, pp. 418-428
- Willert CE, Gharib M (1991) Digital Particle Image Velocimetry. *Exp Fluids*, 10, pp. 181-193
- Wurm F-H. (2004). Systemintegration von Pumpen. Proc. Pumpentagung Karlsruhe, Karlsruhe, VDMA, Germany